Realistic master equation modeling of relaxation on complete potential energy surfaces: Kinetic results

Keith D. Ball
Department of Physics and The James Franck Institute, The University of Chicago, Chicago, Illinois 60637

R. Stephen Berry
Department of Chemistry and The James Franck Institute, The University of Chicago, Chicago, Illinois 60637

(Received 6 May 1998; accepted 14 August 1998)

Using the potential surface information for $(KCl)_5$ and Ar_9 and partition function models introduced in the preceding paper [Ball and Berry, J. Chem. Phys. **109**, 8541 (1998)] we construct a stochastic master equation for each system using Rice–Ramsperger–Kassel–Marcus (RRKM) theory for transition rates between adjacent minima. We test several model approximations to reactant and transition-state partition functions by comparing their master equation predictions of isothermal relaxation for $(KCl)_5$ and Ar_9 with the results of molecular dynamics simulations of relaxations performed in the canonical ensemble. Accurate modeling of the transition-state partition functions is more important for $(KCl)_5$ than for Ar_9 in reproducing the relaxation observed in simulation. For both systems, several models yield qualitative agreement with simulation over a large temperature range. This full treatment of small systems using realistic partition function models is a necessary first step in the application of the master equation method to larger systems, for which one can only expect to have statistical samples of the potential energy surfaces. © *1998 American Institute of Physics.* [S0021-9606(98)02343-5]

I. INTRODUCTION

Many types of clusters can exhibit glassy behavior similar to that of highly amorphous bulk glasses; they take on rather rigid, disordered structures at low temperatures that do not correspond to the thermodynamic ground states.[1,2] However, some types of clusters find ordered, low-energy states even upon extremely fast cooling. An example is the alkali halide clusters, which simulations have shown to be trapped in glassy states only if they are subjected to cooling rates above 10^{13} K/s.[3,4] In general, the minimum cooling rate needed to trap a cluster (or bulk substance) in a glassy state tends to increase with the range of interaction between the system's constituents.[4] The effect of the interaction range on relaxation to the ground state can be understood by examining the system dynamics on its energy landscape, which is itself a consequence of the interaction in question.

The landscape picture of relaxation has been extensively used in the analogous problem of protein folding, albeit more often metaphorically than explicitly. One approach to understanding how proteins are able to find their native state in a feasible amount of time involves the statistical description of the free energy landscape,[5] which originates from the theory of spin glasses.[6] In the context of this topographical viewpoint, protein folding studies have introduced the concept of a ''folding funnel,'' or basin formed by pathways leading to the native state.[5,7–11] For a free energy surface with only one such basin, the native state is kinetically inevitable. A surface with many basins of low free energy, however, has many different and well-separated deep minima. On such a surface, the likelihood of relaxation to one specific minimum or basin may be extremely small.

An alternative approach to studying relaxation on a complex, multidimensional topography starts with the potential energy surface (PES) instead of the free energy surface. The topography can be mapped and characterized by examining sequences of connected minima on the PES. As discussed in the preceding paper,[12] which we will call Paper I, several studies[2,11–13] have delineated the basin structures of several potential surfaces using ''monotonic sequences'' of geometrically linked stationary points. The average energy change between adjacent minima along the monotonic sequences of a specific basin indicates the average energy gradient of that basin. Any basin with a steep average energy gradient may play the role of a ''funnel'' or ''staircase'' discussed in the context of protein folding. However, if the saddles between successive minima are high relative to this energy gradient, they should also be taken into consideration to avoid a misleading picture of the system topography and dynamics. We prefer the term ''basin'' to ''funnel'' because of the strong suggestion the latter carries of a sharply narrowing topography with a very localized minimum—a suggestion which may be premature, in light of a recent study that found low-temperature interconversions on the carboxymyoglobin (MbCO) PES.[16]

By studying the evolution of morphology and the particle movements during downhill moves along such monotonic sequences, one can identify the mechanisms involved in the nucleation and growth of ordered, phaselike forms, and distinguish the characteristics of glass-forming systems from those that can properly be called ''structure-seekers.'' This type of study has been carried out for clusters[2] as well as for a bead model of a polypeptide.[11] Doye and Wales have

conducted such an investigation for a ''hypothetical'' PES,[17] and have examined how the configurational entropy, the number of basins, and the potential energy gradient of basins (determined by trends in the transition barrier heights along monotonic sequences) affect relaxation behavior.

These PES studies led to a master equation approach that links the surface topography to the dynamics on that surface.[13–15,17] In the context of transition-state theory, the matrix of rate coefficients in the master equation embodies the entropic contributions to the free energy, obviating the need to calculate free energies explicitly. This method allows us to study the time evolution of the cluster toward equilibrium. By examining the eigenvalues of relaxation modes for intra- and inter-basin flows, we can infer the effects of multiple PES basins on the system's progress toward equilibrium.[14] Being free to vary the temperature history of such a process, one may determine optimal cooling schedules for approaching target distributions of final energy and morphology of an ensemble of clusters.[18] Such knowledge may be useful for the preparation of clusters with desired mechanical, structural, or electronic properties.

Using the PES information obtained for $(KCl)_5$ and Ar_9 in Paper I, we determine RRKM transition rates for the transitions between adjacent local minima on the surfaces and use these rates to construct a master equation for each system. We then solve the master equations for several temperatures. We employ the models introduced in that paper to calculate the transition rates that enter into the master equation. For the calculation of transition-state partition functions, we use analytic approaches, involving harmonic and anharmonic corrections, as well as a numerical evaluation by integration over normal-mode directions from the transition state. We then compare the time-dependent occupation probabilities of selected minima $P_i(t)$, the mean quenched energy $\langle E_q(t)\rangle$ of occupied minima, relaxation modes, and frequency distributions of the master equation solutions to the results of canonical-ensemble molecular dynamics (MD) relaxation processes. In addition, we analyze the clustering of minima on the potential surfaces in order to determine the hierarchy with which minima merge to form effective catchment basins at various temperatures, elucidating the kinetic consequences of the PES topography.

II. CONSTRUCTING THE MASTER EQUATION

A topographic network like those we have found in Paper I, combined with a transition rate theory to calculate the transition probability for inter-well passage on this network, provides the requisite dynamical information about the flows of arbitrary population distributions on the potential energy surface. This description of the PES lends itself naturally to the stochastic master equation formalism.[19] The master equation is an initial value problem whose solutions $P_i(t)$ are the time-dependent occupation probabilities for each state i of a system. The master equation is a set of coupled rate equations, analogous to the coupled equations for the time variation of concentrations of several chemical species. It has been used to study structural relaxation processes in macromolecules, particularly the folding of lattice models of proteins[5] and heteropolymers,[20] and has played a role in theoretical studies of biased random energy landscapes relating to the glass transition and the folding of proteins.[21,22] It has also been applied recently by Becker and Karplus[23] to the relaxation of the IAN tetrapeptide, based on the PES obtained by Czerminski and Elber.[24,25] Here, we apply the master equation method for the clusters $(KCl)_5$ and Ar_9, studied in Paper I, both to test the validity of various approximations used in the master equation, and to lay the groundwork for using master equations for larger systems, including nanoscale materials and proteins. We use as a criterion of merit the extent to which the results from the master equation agree with the outcome of isothermal MD.

A. Inter-well transition rates

In this work we evaluate inter-well transition rates using RRKM theory.[26,27] The transition probability W_{ij} for passage from well j to well i is the sum of the RRKM transition rates for each of the ''parallel'' $N_{ij}^{\dagger}$ transition states l connecting well j and well i $(i\neq j)$:

$$W_{ij}\equiv k^{j\to i}(\beta)=\sum_{l=1}^{N_{ij}^{\dagger}} k_l^{j\to i}(\beta)$$

$$=\frac{1}{\beta h}\sum_{l=1}^{N_{ij}^{\dagger}}\frac{Z_l^{\dagger}}{Z^{\mathrm{M}}{}_j}\exp(-\beta\Delta V_l). \tag{1}$$

Here $\beta=1/k_BT$ and $\Delta V_l=V_l-V_j$ is the barrier height of the transition, where V_l and V_j are the potential energies of the transition state l and minimum j, respectively. $Z^{\mathrm{M}}{}_j$ and $Z_l^{\dagger}$ are the vibrational partition functions for local minimum j and the transition state l, respectively. The W_{ij} thus defined comprise the elements of the transfer matrix W. The master equation for the time-dependent probability vector $\mathbf{P}(t)$ [whose components are the N_M values $P_i(t)$, the probability of the system residing in well i at time t] is the system of coupled rate equations

$$\frac{dP_i(t)}{dt}=\sum_{j\neq i}[W_{ij}P_j(t)-W_{ji}P_i(t)]. \tag{2}$$

Note that there are no degenerate contributions in this formalism; that is, transitions between potential wells of equivalent geometry (either to the same well or to a permutational isomer) do not affect the ensemble population of this geometry, and so are not counted. In order to write Eq. (2) in matrix form, we take each diagonal element W_{ii} to be the combined rate for all transitions out of well i into wells connected to it:

$$W_{ii}=-\sum_{j\neq i}W_{ji}. \tag{3}$$

Our system of equations can now be written as a linear matrix equation:

$$\dot{\mathbf{P}}(t)=\mathbf{W}\mathbf{P}(t). \tag{4}$$

For a master equation to be linear, its dynamics must be Markovian. That is, the transition rate must depend only upon the current reactant state and the associated transition state or states, and not on which states were visited previ-

ously or on which transition was made to bring the system to its current state. For Markovian dynamics to hold, the vibrations of the reactant state must thermalize before each new transition takes place; any excess kinetic energy deposited in a few hot modes by the previous transition must be redistributed among all modes. We will later examine the validity of the Markovian assumption when discussing simulation results.

B. Solution of the master equation

In order to ensure that $\mathbf{W}$ has a spanning set of eigenvectors with real eigenvalues, it must be symmetrized. To effect a symmetry transformation, we evoke the condition of detailed balance:

$$W_{ij}\sqrt{\frac{P_j^{\mathrm{eq}}}{P_i^{\mathrm{eq}}}}=W_{ji}\sqrt{\frac{P_i^{\mathrm{eq}}}{P_j^{\mathrm{eq}}}}, \tag{5}$$

where P_i^{eq} is the equilibrium (i.e., infinite time) solution of the master equation for $P_i(t)$, given by the usual Boltzmann distribution [Eq. (1) of Paper I]. This equation demonstrates that the transformation $\tilde{\mathbf{W}}=\mathbf{S}^{-1}\mathbf{W}\mathbf{S}$, with transformation matrix $\mathbf{S}=\mathrm{diag}\{\sqrt{P_i^{\mathrm{eq}}}\}$, yields a symmetric matrix. The eigenvalues λ_k of $\tilde{\mathbf{W}}$ are identical to those of $\mathbf{W}$, and its eigenvectors $\tilde{\mathbf{u}}^k$ are related to the corresponding eigenvectors $\mathbf{u}^k$ of $\mathbf{W}$ via the transformation matrix

$$\tilde{\mathbf{u}}^k=\mathbf{S}^{-1}\mathbf{u}^k. \tag{6}$$

This relationship allows the recovery of individual components of the original eigenvectors $\mathbf{u}^k$ in the form $u_i^k=\tilde{u}_i^k\sqrt{P_i^{\mathrm{eq}}}$.

To solve the master equation, the $\tilde{\mathbf{W}}$ matrix is calculated for a given temperature and then diagonalized to yield the eigenvalues λ_k and eigenvectors $\tilde{\mathbf{u}}^k$ that represent the relaxation modes of the system. The general time-dependent solution for $P_i(t)$ can be written as a linear combination of the $\tilde{u}^k$:

$$P_i(t)=\sqrt{P_i^{\mathrm{eq}}}\sum_k c^k\tilde{u}_i^k\exp(\lambda_k t), \tag{7}$$

where we have used the component form of Eq. (6). The overlap of the eigenvector $\tilde{\mathbf{u}}^k$ with the initial probability vector $\mathbf{P}(t=0)$ is given by

$$c^k=\sum_{j=1}^{n}\frac{\tilde{u}_j^k P_j(0)}{\sqrt{P_j^{\mathrm{eq}}}}. \tag{8}$$

The largest eigenvalue is $\lambda_1=0$, and its corresponding eigenvector is given by $\tilde{\mathbf{u}}^1=\sqrt{\mathbf{P}^{\mathrm{eq}}}$. Since all other eigenvalues are negative, their corresponding modes are the transient ''relaxation'' modes. Hence, the solution that remains as $t\to\infty$ is precisely the Boltzmann equilibrium probability $\mathbf{P}^{\mathrm{eq}}$. For the general class of initial conditions, the Boltzmann solution will only be attained in the long-time limit for nondecomposable transfer matrices which correspond to connected potential surfaces. Since all minima in the clusters we study are connected to each other via a sequence of transition states, all transfer matrices we obtain will be nondecomposable.

III. RELAXATION PROFILES

We can now use our models for the partition functions in Eq. (1) to predict the stochastic evolution of $(KCl)_5$ and Ar_9 during a canonical-ensemble relaxation process. In order to test the model used for the saddle partition functions, we compared the theoretical predictions for relaxation to the same process simulated by MD. Our models are referred to by the following nomenclature: (Z^{M})-$(Z^{\dagger})$, where ''Z^{M}'' is the code for the model used to approximate the catchment basin partition functions, as given in Table II in Paper I. Specifically, the models retained from Paper I for kinetic analysis are these: the Morse barrier methods MB($\eta_{\mathrm{P}}=0.1$) and MB-S, which use a Morse anharmonicity approximation based on actual transition barrier energies, the harmonic partition function approximation (H), and the ''transition state valley'' (TSV) models, which add approximate contributions to the canonical density of states due to the TSV regions along reaction paths near the transition states. These models either approximate the potential energy along the reaction coordinate as constant or ''flat,'' (FTSV), or evaluate it and integrate the partition function contribution numerically (ITSV). The TSV models have an additional indicator (''/H'' or ''/N'') indicating the approximation scheme of $Z^{\dagger}$ used in the model [see Eq. (11) of Paper I]. ''$Z^{\dagger}$'' consists of a single letter, indicating whether an harmonic (H), numerical (N), or Taylor (T) approximation is used to evaluate the $Z^{\dagger}$, as defined in Paper I.

For both $(KCl)_5$ and Ar_9 we present the results from temperatures below, within, and above the solid–liquid coexistence region. Above the coexistence region, the systems are effectively liquidlike. In this range, anharmonicities are important, and there is the possibility that reactant states might not equilibrate before a transition is made, breaking down the Markovian assumption. For $(KCl)_5$, there is evidence that some transitions from high-energy minima in the liquid range may occasionally occur within a few mean normal-mode vibration periods, $\tau_{\mathrm{mean}}=3.5\times10^{-13}$ s. Since no one minimum at high energies has a large probability in either system, this behavior is not likely to have a significant correlated influence on an ensemble of relaxations. Moreover, the relaxation from high-energy to lower-energy configurations occurs rather quickly, and never seems to be rate limiting; the subsequent transitions between the lower-energy minima, where RRKM theory is more reliable, will inevitably dominate all but the first instants of the relaxation process.

The higher dimensionality of larger systems, which will be of interest for applications to nanoscale particles and proteins, means that these systems will involve larger numbers of coupled modes, and will allow for smoother, and possibly more rapid equilibration. This assumption is borne out by simulations of $(KCl)_{32}$ and Ar_{55} which show that the time between transitions during relaxation from all but the highest-energy configurations is at least on the order of hundreds of normal-mode vibration periods, which is likely sufficient to guarantee equilibration.[28]

A. $(KCl)_5$

For $(KCl)_5$, we perform relaxation at the following temperatures, which represent the three temperature regimes discussed above: (1) 400 K, (2) 500 and 520 K, and (3) 800 K. First, we focus on the time evolution of the occupation probabilities $P_i(t)$ for the global minimum and rectangle (minima 1 and 4, respectively), for processes which begin in the decagon: $P_8(t=0)=1$. Since there is only one transition state out of the decagon (to the rectangle), this rate can be compared directly to the slope of $\log P_8(t)$. The simulations were performed with time step $\tau=2$ fs. Each simulation began with an initial short interval during which the system could distribute energy into its vibrational modes. At 400 K and 500 K, the system was then quenched at intervals of 1 ps for 2000 intervals. At 800 K, 1000 quenches at 0.25 ps intervals were performed. The quench results were averaged over 200 simulations and binned according to the local minimum found at each quench interval.

The resulting $P_i(t)$ are plotted in Fig. 1 at 400 K, 500 K, and 800 K. The simplest model, using harmonic theory for both Z_i and $Z_i^{\dagger}$ (H-H), clearly has too short a relaxation time scale. To explore the effects that the $Z^{\dagger}$ have on the results, we employ the H-N model. We note that this model slows the relaxation time scales, improving their agreement with simulation markedly. Slower relaxation is consistent with Eq. (1) and the observation in Paper I that numerical approximations of $Z^{\dagger}$ tend to be smaller than their harmonic approximations. Paper I also notes that the FTSV/H model is only slightly better overall at predicting simulation values of P^{eq} than the harmonic approximation. Likewise, the $P_i(t)$ profiles we observe here for the FTSV/H-H and FTSV/H-N model are similar to those of H-H and H-N, respectively. We therefore omit these results from Fig. 1.

As shown in Paper I, the MB($\eta_{\mathrm{P}}=0.1$) model gives the correct relative magnitudes of the reactant-state partition functions. Under the assumption that this model also reasonably approximates absolute partition functions, it should provide a reference point for testing the reliability of transition-state partition function models and of RRKM theory itself. As Fig. 1 shows, MB($\eta_{\mathrm{P}}=0.1$)-N agrees very closely with simulation except at 800 K, where the time scale from simulations for populating minima 1 and 4 is about twice as long. The MB($\eta_{\mathrm{P}}=0.1$)-T results, while relaxing on a slightly longer time scale, are almost identical to those of MB($\eta_{\mathrm{P}}=0.1$)-N. Therefore, we can choose either numerical or Taylor approximations for $Z^{\dagger}$ and achieve the same results. However, the time scale of the MB($\eta_{\mathrm{P}}=0.1$)-H results is clearly too short. We conclude that the harmonic approximation overestimates $Z^{\dagger}$, since it predicts too wide a ''mouth'' at the transition state. On the other hand, our numerical and Taylor approximations work quite well. At high temperatures, the relative slowness of the best models may perhaps point to the increasing importance of higher-rank transition states (those with more than one imaginary normal-mode frequency), which account for faster MD relaxation. In Paper I, the best analytic alternative to MB($\eta_{\mathrm{P}}=0.1$) proved to be MB/S. In Fig. 1, MB/S-N matches the behavior of MB($\eta_{\mathrm{P}}=0.1$)-N quite closely, except at 800 K. Overall, this model also serves as a good model of relaxation.

Although ITSV models did not perform well in Paper I, we compared their kinetic predictions to the better models to determine the sensitivity of the relaxation time scales to model choice. Even though the fitness of ITSV/H is somewhat better than that of ITSV/N at high temperatures, both are equally poor at modeling kinetic behavior in this region, yielding much slower relaxation than the simulations or other models. This slowness likely indicates that these models give partition functions for the local minima that are systematically too large. At and below the coexistence region, ITSV/H relaxation profiles are far slower, and approach asymptotic values that are vastly different from those of all other models. For this reason, we omit the results of this model from Fig. 1. This pathological behavior is a reflection of Paper I results, in which ISTV/H proved to be highly inaccurate for low temperatures, and unusable below 350 K. On the other hand, at the coexistence region and lower, ITSV/N-N is nearly a viable model (see Fig. 1). Neither, however, is a suitable model in general.

We illustrate the evolution from the initial state (minimum 8) by examining the transition rate $k^{8\rightarrow 4}$, shown in Fig. 2. It is apparent that numerical evaluation of $Z^{\dagger}$ brings the rates into quite good agreement with the rates observed from simulation, and that the discrepancies between these models are smaller than with respect to harmonic $Z^{\dagger}$ models, whose rates are characteristically too high. Having confidence in the accuracy of the numerical $Z^{\dagger}$ model, we can test our suspicion that Z^{M} is overestimated by ITSV models. The inaccuracy of the ITSV/N-N model is manifest for very high temperatures, where the rate for the $8\rightarrow 4$ transition actually decreases. For ITSV/H-N, the rate is depressed over the whole temperature range. In both cases, the approximations to Z^{M} are clearly too large.

Our detailed examination of relaxation on the level of individual minima has enabled us to evaluate the performance of various models for $Z^{\dagger}$. However, this test only shows the behavior within specific minima, starting from specific initial conditions. To obtain a simpler, comprehensive picture of how relaxation on the PES progresses, we use the average quenched energy $\langle E_q(t)\rangle$ to describe the global topographical state of our system as a function of time. This ensemble average may be written in terms of the probability weights $P_i(t)$ given by Eq. (7):

$$\langle E_q(t)\rangle = \sum_i V_i P_i(t) = \sum_i V_i \left(\sum_k \sqrt{P_i^{\mathrm{eq}}} c^k \tilde{u}_i^k \exp(\lambda_k t) \right). \tag{9}$$

Here, V_i is the potential energy of minimum i and c^k is the overlap coefficient given by Eq. (8). By reversing the order of summation, we can write this quantity in terms of the relaxation modes:

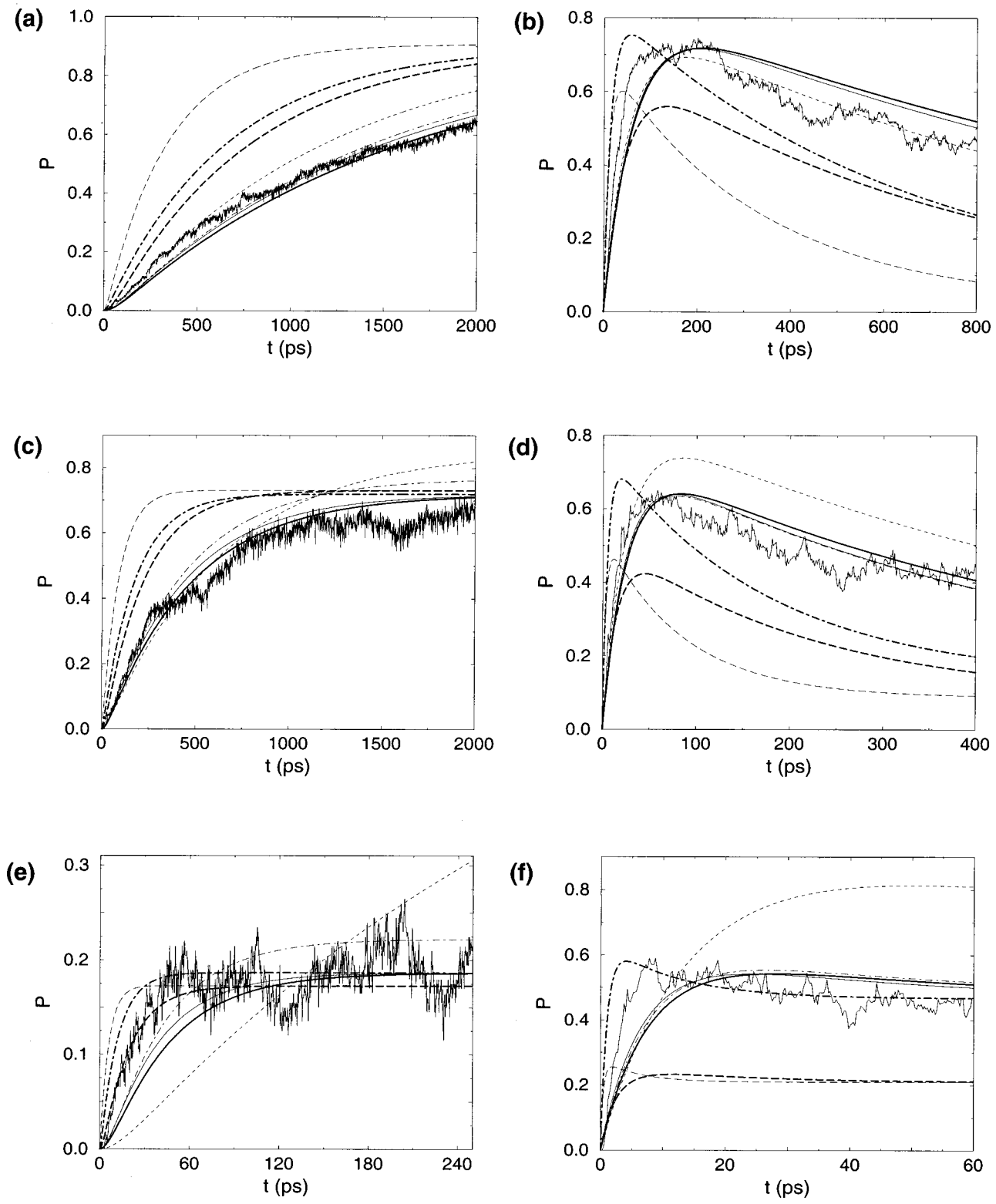

FIG. 1. $(KCl)_5$ relaxation profiles $P_i(t)$ for (a) $i=1$ and (b) $i=4$ at 400 K, (c) $i=1$ and (d) $i=4$ at 500 K, (e) $i=1$ and (f) $i=4$ at 800 K. MD results are represented by the jagged line; models are indicated by: H-H—thin long dashes; H-N—thick long dashes; MB/S-N—thin dot-dashed line; MB($\eta_P=0.1$)-H—thick dot-dashed line; MB($\eta_P=0.1$)-N—thin solid line; MB($\eta_P=0.1$)-T—thick solid line; ITSV/N-N—thin short dashes.

$$\langle E_q(t)\rangle = E_q^{\mathrm{eq}} + \sum_{k=2}^{N_M} A^k \exp(\lambda_k t). \tag{10}$$

We can now view the relaxation profile $\langle E_q(t)\rangle$ as the equilibrium baseline E_q^{eq} plus a series of decaying exponential modes with amplitudes

$$A^k = c^k \left(\sum_i \sqrt{P_i^{\mathrm{eq}}} V_i \tilde{u}_i^k \right). \tag{11}$$

Using this spectral decomposition, we can extract both the relaxation time scales and their relative importance (represented by the A^k) from the simulation data by fitting it to

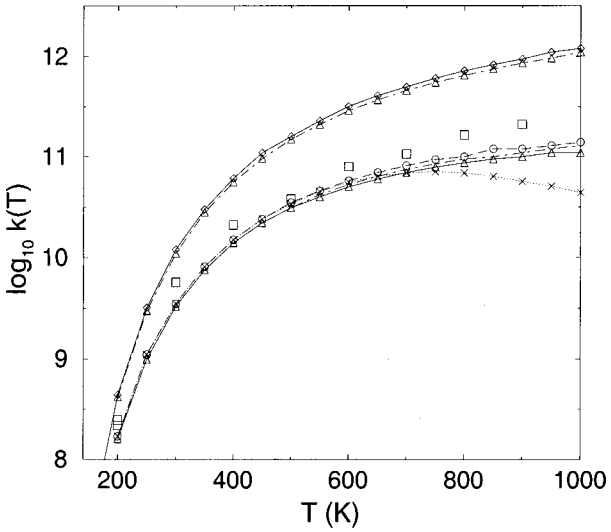

FIG. 2. Temperature dependence of the decagon-to-rectangle rate $k^{8\to4}$. MD results are indicated by squares. There are two main bands formed by the models. Two harmonic $Z^{\dagger}$ models form a high-rate band: H-H—solid line/diamond; MB($\eta_P=0.1$)-H—dot-dashed line/triangle; the following three numerical $Z^{\dagger}$ models form a lower, more accurate band: H-N—dashed line/circle; MB/S-N—solid line/triangle; MB($\eta_P=0.1$)-N—dot-dashed line (between the H-N and MB/S-N lines). The dotted line/'X' data are for the ITSV/N-N model.

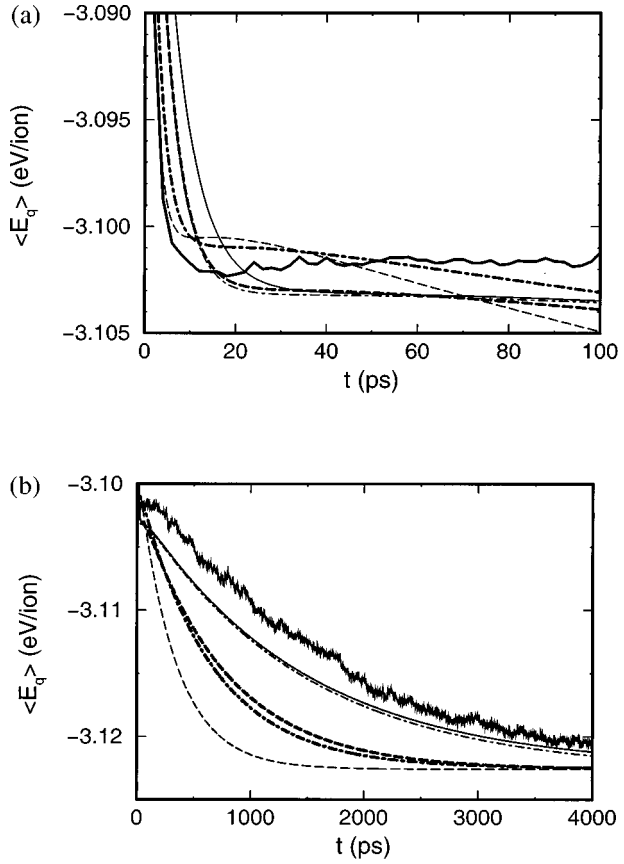

FIG. 3. $\langle E_q(t)\rangle$ profile at 400 K starting from minimum 12 of $(KCl)_5$. Shown are the (a) intermediate and (b) long time scales. MD results are represented by the jagged line; models are represented as follows: MB($\eta_P=0.1$)-N—thin solid line; MB/S-N—thin dot-dashed line; MB($\eta_P=0.1$)-H—thick dot-dashed line; H-H—thin dashed line; H-N—thick dashed line.

some number of terms of Eq. (9). These quantities can be directly compared with the eigenvalue spectrum and corresponding amplitudes that result from the transfer matrix representing a given model. In practice, we were able to resolve two to three (and in one instance, four) eigenvalues λ_k, and their corresponding amplitudes A_k, from the relaxation scenarios.

To obtain E_q^{eq}, we use Eq. (8) and the fact that $\lambda_1=0$ and $\tilde{\mathbf{u}}^1=\sqrt{\mathbf{P}^{eq}}$ to obtain the expected ensemble probability expression:

$$E_q^{eq}=A^1=\sum_i V_i P_i^{eq}. \tag{12}$$

Model E_q^{eq} values can then be compared directly to the simulation value, which can be calculated from the P_i^{eq} obtained at equilibrium, or obtained directly from asymptotic values of $\langle E_q(t)\rangle$ observed at long relaxation times.

We obtained $\langle E_q(t)\rangle$ profiles for $(KCl)_5$ by running a new set of MD trajectories at 400 K, 520 K, and 800 K, starting from minima 12, 19, and 22 (the highest-energy minimum). From each minimum, 400 runs were initiated, with a typical quenching frequency of 2000 quenches per run. The interval between quenches was chosen so that the total length of the run would be sufficient to establish the equilibrium baseline E_q^{eq}. At 400 K, this interval length was 2 ps when starting from minima 12 and 19, for a total length of 4000 ps, and 0.4 ps when starting from minimum 22, for a total length of 800 ps. At 520 K, we used a quench interval of 200 ps, with a total simulation length of 2000 ps. At 800 K, we found that using a quench interval of 20 fs, with a total length of 40 ps, was sufficient.

For $\langle E_q(t)\rangle$ profiles at 400 K starting from minimum 12 (Fig. 3) and minimum 19 (not shown, but similar to the minimum 12 case), there are three characteristic time scales. From minimum 12, the first is a fast decay to an intermediate energy of -3.102 ± 0.001 eV/ion in the first 15 ps. This time is consistent with the $12\to4$ reaction, which for the H-H model has a rate of 8×10^{11}/s. The second time scale is the dwell time the system spends at the intermediate-energy region, chiefly due to a ''reservoir effect'' caused by minimum 4. This energy is slightly lower than that of minimum 4(-3.0979 eV/ion), due to series of transitions such as $12\to10\to14\to1$, whose individual rates are of the same order as the $12\to4$ rate. These alternate channels allow some of the occupation probability to accumulate in the global minimum during the fast time scale. The second time scale ranges from 200 ps in length for MD, to as short as 20 ps for the harmonic $Z^{\dagger}$ family of models. The third and longest time scale involves the asymptotic relaxation to E_q^{eq} and is an order of magnitude longer than the intermediate scale. Two aspects of PES connectivity cause this slow relaxation. First, the transition state $4\to1$, with rate $k^{4\to1}\approx5\times10^9$/s, is the only path between minimum 4 and and the basin of low-energy three-dimensional structures (1, 2, 3, 5, 6, 7) mentioned in Paper I and in the section on PES basin structures below. The relaxation time is further slowed by competing transitions from the global minimum to minima 2 and 3.

In Fig. 3 we plot the simulated $\langle E_q(t)\rangle$ for relaxation from minimum 12. For comparison, we plot MB($\eta_P = 0.1$)-N as the best candidate model. We also include MB($\eta_P = 0.1$)-H, to illustrate the effect of using different $Z^\dagger$ models with the same Z^M model. We also include the simplest model H-H along with H-N, to gauge the extent of improvement, if any, that the numerical $Z^\dagger$ model makes. In addition, we evaluate the performance of MB/S-N, since MB/S proved to be the best fully analytic alternative to MB($\eta_P = 0.1$) in Paper I.

On the fast time scale, models employing harmonic $Z^\dagger$ yield faster transitions and follow the MD curve more closely, while the corresponding models using numerical $Z^\dagger$ are slower by as much as a factor of 2. Over this time scale, models H-N and MB/S-N are essentially identical. The corresponding harmonic models H-H and MB($\eta_P = 0.1$)-H also share similar profiles. This relative insensitivity of the fast time scale to choice of Z^M model emphasizes that the various models make little if any change in minimum 12, since the models were chosen to optimize the accuracy of Z^M for minima with higher P^{eq}. This rapid energy drop at early times is analogous to the fast collapse of proteins to a compact state. In the case of $(KCl)_5$, this action is the fast collapse to a highly ordered, planar metastable state (the rectangle), followed by slow relaxation to the global minimum.

The harmonic $Z^\dagger$ models arrive at the ''collapsed'' phase faster than numerical $Z^\dagger$ models, and result in dwell times approximately one-fifth of those of the numerical models. The longer time scale of numerical $Z^\dagger$ affords stabilization at a lower intermediate potential energy. It is in the longer second and third post-collapse time regions that differences between models become important for relaxation. As previously observed, harmonic $Z^\dagger$ models yield significantly shorter relaxation time scales than those observed for MD. In the relaxation plot over the entire relaxation [Fig. 3(b)], the numerical $Z^\dagger$ models MB($\eta_P = 0.1$)-N and MB/S-N more faithfully reproduce the long MD time scale. The results of these two models and the MB-T model (which, for clarity, we omit), are in fact quite similar. As a class, these MB models yield the best overall agreement to the simulated relaxation profile, with their $\langle E_q(t)\rangle$ curves just within the typical error in the MD relaxation profile. It is instructive to note that the differences between MB($\eta_P = 0.1$) and MB/S results are much smaller than differences between the harmonic and the numerical or Taylor-approximated $Z^\dagger$ models. We reinforce this observation by noting that H-N makes a significant improvement over H-H. Conversely, MB($\eta_P = 0.1$)-H performs considerably worse than either MB($\eta_P = 0.1$)-N or MB/S-N, due to its higher values of $Z^\dagger$.

Relaxation from minimum 19 (not shown) is similar to relaxation from minimum 12, exhibiting the same three fundamental time scales and relative model behaviors. On the intermediate time scale, all models reach intermediate energies that are slightly higher than the MD value. On the long time scale, MB($\eta_P = 0.1$)-N and MB/S-N agree with the MD profile slightly better than in the profiles starting from minimum 12. Likewise, relaxation from the same minima at 520 K exhibits a similar $\langle E_q(t)\rangle$ profile and much the same relative model behavior, as shown in Fig. 4(a) for profiles starting from minimum 12. At this temperature, the long time scales have shortened by nearly a factor of 10.

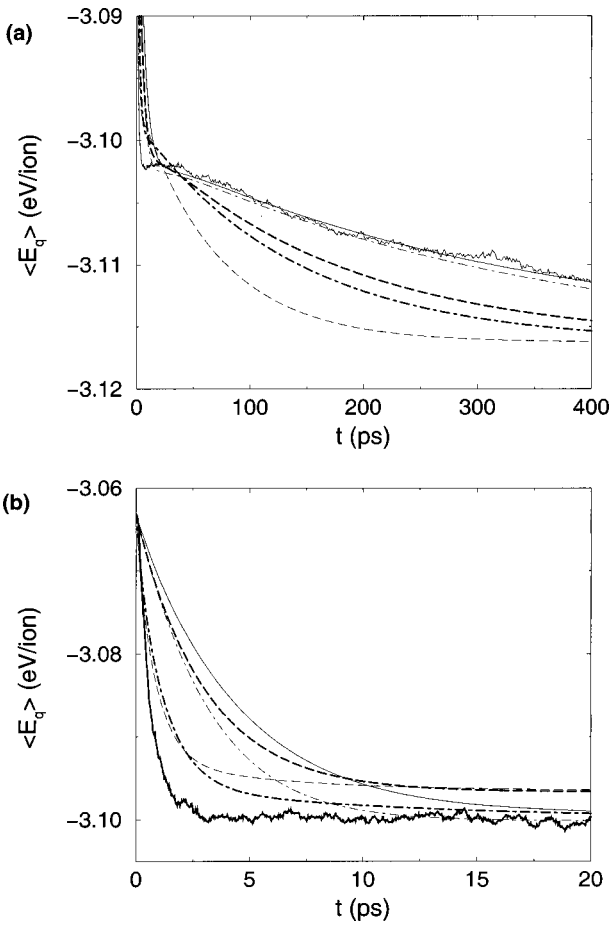

FIG. 4. $\langle E_q(t)\rangle$ profile starting from minimum 12 of $(KCl)_5$ at (a) 520 K and (b) 800 K. MD results are represented by the jagged line; models are represented as follows: MB($\eta_P = 0.1$)-N—thin solid line; MB/S-N—thin dot-dashed line; MB($\eta_P = 0.1$)-H—thick dot-dashed line; H-H—thin dashed line; H-N—thick dashed line.

At 800 K [Fig. 4(b)], only the fast decay from the initial states is evident, since the global minimum is no longer favored at equilibrium. At 800 K, $E_q^{eq} = -3.0997$, and minimum 4 is occupied with probability 0.46. Hence the fast, direct transitions to minimum 4 bring the system close to the equilibrium distribution. At this temperature, the apparently better accuracy of the harmonic $Z^\dagger$ models is fortuitous. During the fast decay, the system is on the boundary of the ergodicity assumption of RRKM, and is in a temperature regime for which higher-rank transition channels are likely to become important. These factors would tend to increase the real transition rate with respect to RRKM theory. We then expect all of our models to relax more slowly in the collapse phase than does the real system, with the harmonic $Z^\dagger$ models being characteristically faster than numerical $Z^\dagger$ models.

Relaxation from minimum 22 exhibits fundamentally different profiles at 400 K [see Fig. 5(a)], since a direct ''collapse'' channel $22 \rightarrow 1$ exists with rate $k^{22\rightarrow 1} \approx 2 \times 10^{11}$/s which dominates the only other channel (through minimum 20). The relaxation time scale in this case is 5 ps for simu-

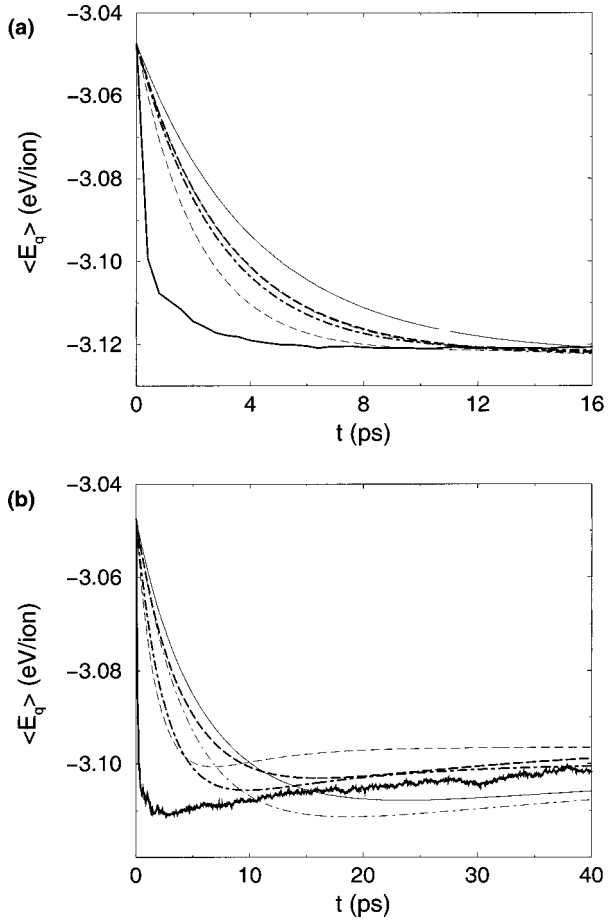

FIG. 5. $\langle E_q(t)\rangle$ profiles starting from minimum 22 of $(KCl)_5$ at (a) 400 K and (b) 800 K. Models are represented as follows: MB($\eta_P=0.1$)-N—thin solid line; MB/S-N—thin dot-dashed line; MB($\eta_P=0.1$)-H—thick dot-dashed line; H-H—thin dashed line; H-N—thick dashed line.

lation, and 10–15 ps for model results. As in the case of minima 12 and 19 at 800 K, harmonic $Z^\dagger$ models relax faster than numerical $Z^\dagger$ models on the fast time scale, with all models yielding slower relaxation than simulation, due to suspected violations of RRKM theory. Since the fastest channel from minimum 22 leads to minimum 1, and not minimum 4, $\langle E_q(t)\rangle$ first takes a downward dip toward the global minimum energy at 800 K, before slowly increasing to E_q^{eq}. In this case, the models have similar problems as do fast transitions at higher temperature [see Fig. 5(b)].

We have found that the eigenvalues obtained by fitting Eq. (9) to the data yield the same picture of model performance that we obtained by qualitative inspection of relaxation profiles. However, these eigenmodes are instance specific; that is, they are not only dependent on T, but on the initial occupation probability distribution. To provide a picture of how the solutions of the master equation change with temperature that is independent of initial conditions, we give histograms of the 21 nonzero eigenvalues of the MB($\eta_P=0.1$)-N model transfer matrix in Fig. 6(a). Other models of at least moderate accuracy produce distributions similar to those given in the figure. In addition, eigenvalues for this model at the temperatures of the $\langle E_q(t)\rangle$ data are given in Table I.

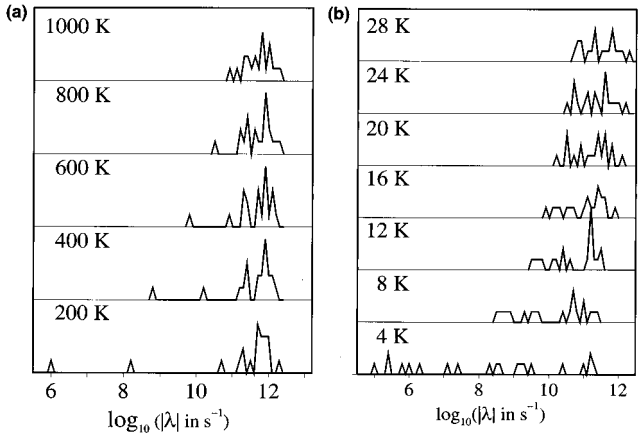

FIG. 6. Histograms of W-matrix eigenvalues λ_k for (a) the MB($\eta_P=0.1$)-N model for $(KCl)_5$ and (b) the MB($\eta_P=0.1$)/S-N model for Ar_9 at a series of temperatures.

At low temperatures, there is a peak of fast eigenvalues at $|\lambda|\approx 10^{12}$ Hz which broadens with increasing temperature. Notably, the largest eigenvalue (fastest mode) of the distribution is nearly independent of temperature. As temperature decreases, the lowest few eigenvalues decrease rapidly in magnitude. The corresponding modes, when they overlap significantly with the initial ensemble distribution, cause the system dynamics to freeze out before reaching the Boltzmann distribution, giving rise to nonergodic dynamics, and possibly glassy behavior. These eigenvalues steadily increase with temperature until they converge with the rest of the distribution at higher time constant. Since the fastest modes typically involve only local transitions, often between only two wells, and the slower modes involve more global probability flow, the convergence of eigenvalues is an indicator that global movements on the PES are occurring almost as quickly as individual transitions, since transition barriers are significantly reduced. Similar eigenvalue convergence has been observed for an Ar_{19} study using a simple Einstein frequency approximation in the transition rate expressions of Eq. (1).[13]

B. Ar_9

For Ar_9, we first focus on the time evolution of the occupation probabilities $P_i(t)$ for the global minimum and minimum 9 for processes which begin in the highest-energy minimum: $P_{21}(t=0)=1$. We choose minimum 9 since it is the most important intermediate state between minimum 21 and the global minimum. The simulations were performed with time step $\tau=3$ fs. As with $(KCl)_5$, we randomly perturbed the initial geometry and allowed the system to thermalize before starting the relaxation process. If the system left the initial state, it was returned at $t=0$. The relaxation profiles were averaged over 200 runs at each temperature. We discuss the results at three temperatures. At 10 K, the system is virtually confined to the global minimum. At 16 K, the rms bond length fluctuation

TABLE I. Spectra of master equation eigenvalue magnitudes in units of ps^{-1}, in order of decreasing value. For each system, one spectrum is taken from the solidlike, coexistence, and liquidlike temperature regimes. The selected temperatures are those at which the $\langle E_q(t)\rangle$ simulation data were obtained.

	$\log_{10}$ (λ in ps^{-1})					
	$(KCl)_5$			Ar_9		
System						
T	400 K	520 K	800 K	10 K	18 K	24 K
	12.2390	12.2100	12.2539	11.4038	11.9799	12.2252
	12.1195	12.0741	12.1551	11.3281	11.7286	11.9587
	12.0775	12.0053	12.0828	11.2408	11.7152	11.9074
	12.0170	11.9486	12.0437	11.2072	11.5636	11.7623
	11.9615	11.9010	12.0246	11.1710	11.5624	11.7296
	11.9081	11.8984	11.9429	11.1430	11.5300	11.6459
	11.9062	11.8972	11.9106	11.0509	11.4816	11.6336
	11.8826	11.8789	11.8558	11.0319	11.4026	11.6213
	11.8756	11.8687	11.8558	11.0003	11.2803	11.6049
	11.8543	11.8456	11.8520	10.9497	11.2665	11.4483
	11.8234	11.8091	11.7899	10.9366	11.2318	11.2853
	11.7502	11.7491	11.7323	10.1691	11.2086	11.2624
	11.6960	11.6701	11.6231	10.1116	11.1020	11.1484
	11.6958	11.6686	11.6199	9.9800	10.7956	11.0980
	11.4203	11.3543	11.4394	9.9674	10.7613	11.0152
	11.4048	11.3489	11.3791	9.6657	10.5889	10.8005
	11.3563	11.2904	11.3514	9.4075	10.4187	10.7316
	11.3296	11.2827	11.3190	9.3348	10.3833	10.7025
	11.2128	11.1076	11.1794	9.2328	10.3192	10.6658
	10.2235	10.6852	11.1607	9.1552	10.1006	10.4796
	8.8407	9.4679	10.4585			

$$\delta = \frac{2}{N(N-1)} \sum_{i<j} \frac{(\langle r_{ij}^2\rangle - \langle r_{ij}\rangle^2)^{1/2}}{\langle r_{ij}\rangle} \tag{13}$$

between the $N=9$ particles starts to increase sharply,[29] indicating that the system particles are making rearrangements. Hence we refer to 16 K as the discontinuity temperature $T_D^{Ar_9}$. These rearrangements coincide with the growth of P^{eq} at this temperature for geometries other than the global minimum. At the third temperature, 24 K, the system still occupies the global minimum a majority of the time, but now clearly exhibits liquidlike behavior. By choosing these temperatures, we are exploring the same regimes as we did with $(KCl)_5$.

In Fig. 7, we plot $P_1(t)$ and $P_9(t)$ for several models along with the simulation results. Compared to simulation, the MB models tend to yield similar, or slightly shorter, relaxation time scales within the global minimum, and somewhat faster time scales in minimum 9. In the latter case, the faster time scale causes $P_9(t)$ to reach values nearly twice as high as the peak probability attained by simulation. This discrepancy decreases at higher temperature. At 10 K, anharmonicities are of little importance, and the various MB models give quite similar results. As expected, this agreement starts to break down at higher temperatures. Counter to the results with $(KCl)_5$, the MB($\eta_P=0.1$)/S-H and -N models are similar at all three temperatures, indicating that for Ar_9, the choice of $Z^\dagger$ model is less important than the choice of Z^M model. Of the MB family, all behave reasonably, but the MB($\eta_P=0.1$) models retain more accurate time scales and P^{eq} values at 24 K. Surprisingly, the MB($\eta_P=0.1$)-N model, while behaving in a fashion similar to MB($\eta_P=0.1$)/S-N around the global minimum, has a $P_9(t)$ profile much closer to the simulation profile. Since MB/S and MB($\eta_P=0.1$)/S only allow anharmonic corrections for low energy minima (up to minimum 9), the partition function for minimum 21 will be smaller, and the corresponding rate 21→(products) will be larger than in the MB($\eta_P=0.1$) model. This feature of the ''/S'' models likely accounts for much of the discrepancy noted for $P_9(t)$.

Although the TA and numerical models produce similar results that reproduce P^{eq} nearly as well as MB($\eta_P=0.1$)/S, they give rise to much faster relaxation than occurs in the simulations, a problem which worsens as temperature increases. Hence these models may only correct the relative magnitude of the Z^M, while underpredicting their absolute size. In a similar fashion, FTSV is worse than the harmonic approximation to P^{eq}, but is surprisingly adept at modeling kinetics. Although its predictions for the global minimum at liquidlike temperatures are poor, it performs better for both minima (especially minimum 9) at 10 and 16 K than the MB models, in accord with its particularly good modeling of P_9^{eq}. Conversely, the ITSV/H-N model, which proved to be the best overall analytic model for P^{eq}, yields relaxation time scales that are far too long, due to the extreme overestimation of Z^M, and will not be considered further. These observations indicate that there may be a trade-off involved when choosing an optimal model for both equilibrium and kinetic predictions.

We next examined $\langle E_q(t)\rangle$ for relaxation at 10, 18, and 24 K, starting from minima 17, 19, and 21. For each temperature and starting minimum, the results are averaged over 400 simulations. In all cases, $\langle E_q(t)\rangle$ consists of a fast initial

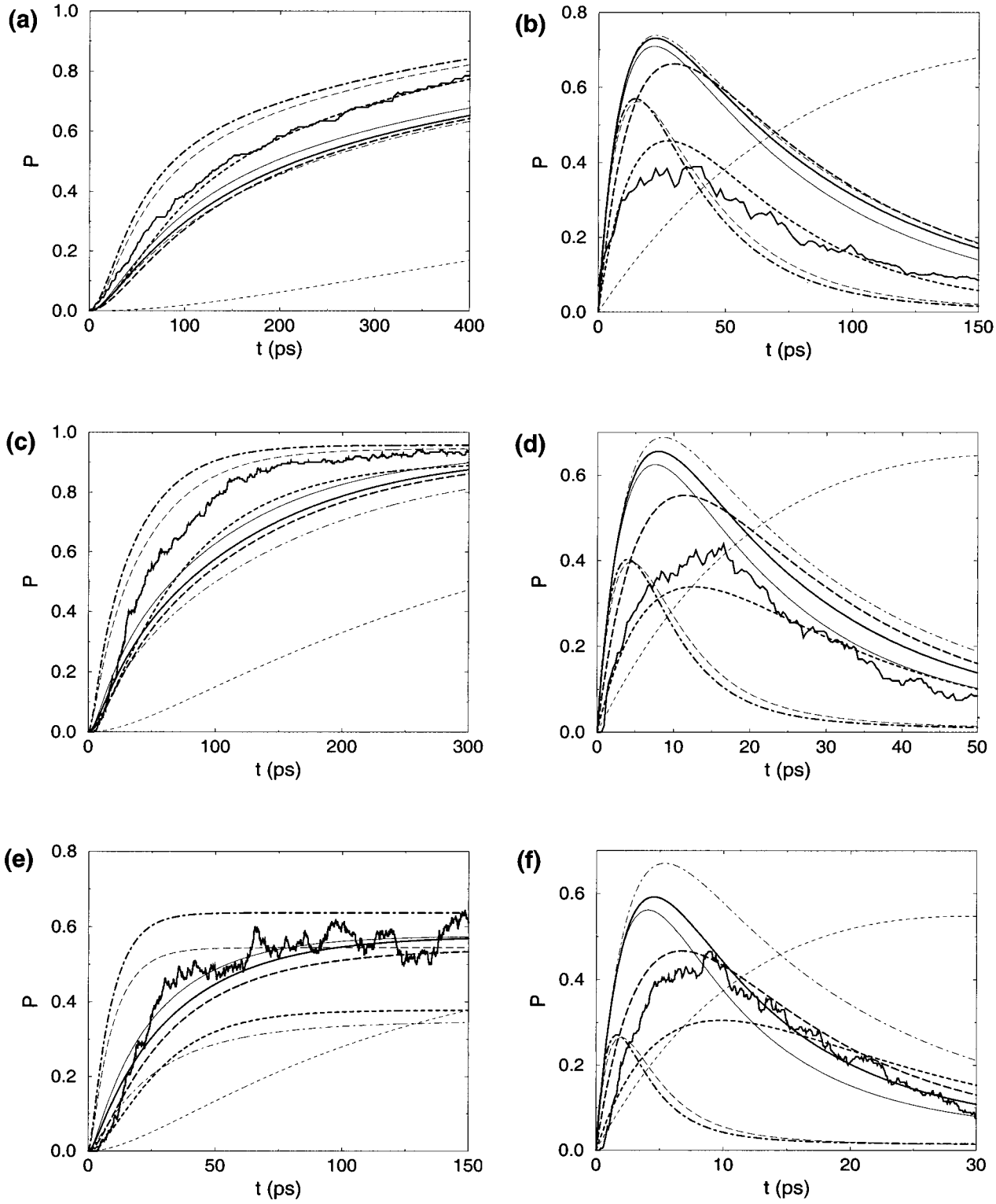

FIG. 7. Ar_9 relaxation profiles $P_i(t)$ for (a) $i=1$ and (b) $i=9$ at 10 K, (c) $i=1$ and (d) $i=9$ for 16 K, (e) $i=1$ and (f) $i=9$ for 24 K. MD results are represented by jagged line; models indicated by: H-N—thin long dashes; MB($\eta_P=0.1$)/S-H—thin solid line; MB($\eta_P=0.1$)/S-N—thick solid line; MB($\eta_P=0.1$)-N—thick long dashes; MB/S-N—thin dot-dashed line; TA-N—thick dot-dashed line; FTSV/H-N—thick short dashes; ITSV/H-N—thin short dashes.

decay, followed by a slower equilibration regime. In some cases, three relaxation modes can be resolved from the data, yet none of the $\langle E_q(t)\rangle$ profiles observed spend an appreciable dwell time at an intermediate energy, as occurred from minima 12 and 19 of $(KCl)_5$. Features of the $\langle E_q(t)\rangle$ profiles observed from simulation and select models are similar to those starting from minimum 21, shown in Fig. 8.

The models MB($\eta_P=0.1$)-N, MB($\eta_P=0.1$)/S-H, and MB($\eta_P=0.1$)/S-N yield very similar profiles at 10 K, and, to a lesser degree, at 24 K. We note that MB($\eta_P=0.1$)/S-H and MB($\eta_P=0.1$)/S-N agree more closely with each other than with MB($\eta_P=0.1$)-N. As noted above, the choice of model

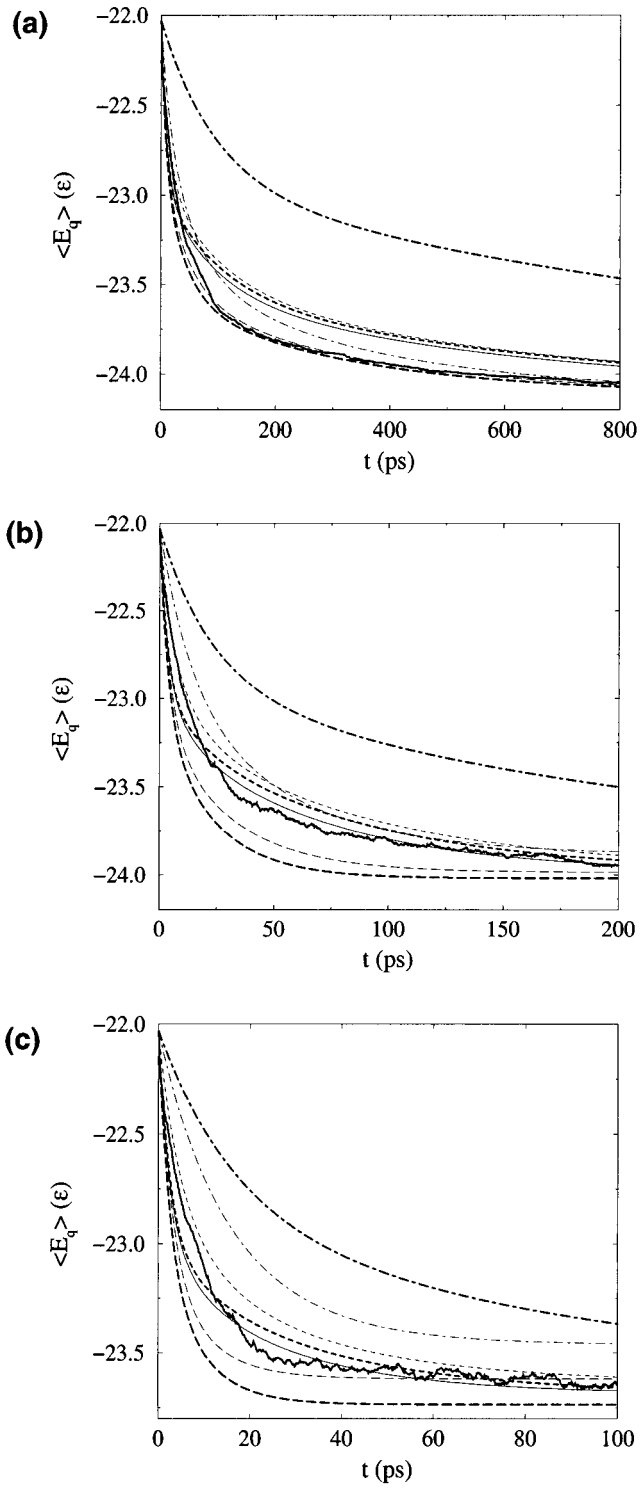

FIG. 8. $\langle E_q(t)\rangle$ profiles starting from minimum 21 of Ar_9 at (a) 10 K, (b) 18 K, and (c) 24 K. MD results are represented by jagged line; models are represented as follows: MB($\eta_P=0.1$)/S-N—thick short dashes; MB($\eta_P=0.1$)/S-H—thin solid line; TA-N—thick long dashes; H-N—thin long dashes; ITSV/H-N—thick dot-dashed line; FTSV/H-N—thin dot-dashed line; MB($\eta_P=0.1$)-N—thin short dashes.

for Z^M tends to be more significant than for $Z^\dagger$. In the $\langle E_q(t)\rangle$ plots, overly rapid relaxation to intermediate energies causes the MB($\eta_P=0.1$)/S models to initially decay too steeply. On the other hand, MB($\eta_P=0.1$)-N has a slower decay, since the latter model includes the reaction-path contributions to the partition function of minimum 21.

As in Fig. 7, the $\langle E_q(t)\rangle$ profiles for H-N and TA-N decay too quickly, with TA-N consistently faster than H-N. At 10 K, however, these models are closer than MB models to the simulation results. When observing the eigenvalue spectra, we will display only the H-N results, which are slightly more accurate than those of TA-N.

As expected, ITSV/H-N produces much slower relaxation than other models, even though its asymptotic E_q^{eq} values are in reasonably good agreement with simulation. FTSV/H-N is much better than the MB models at modeling the initial fast decay, and at 10 K is closer to the simulation profile than are the MB models. However, its prediction of E_q^{eq} becomes progressively too high as temperature increases, since it fails to model the increase in anharmonicity with temperature.

For Ar_9, we were able to resolve either two or three eigenvalues from the simulation data, and found a more quantitative, but similar, picture of the model performance as given by the observed $\langle E_q(t)\rangle$ profiles. In Fig. 6(b) we plot eigenvalue histograms produced by the MB($\eta_P=0.1$)/S-N model, and give the eigenvalues for this model at the same temperatures as the $\langle E_q(t)\rangle$ data in Table I. As for $(KCl)_5$, other reasonably behaved models yield qualitatively similar distributions. As for $(KCl)_5$, the eigenvalue spectrum is concentrated at large time constant values at high temperatures. Unlike $(KCl)_5$, a decrease in temperature results in an almost even distribution of eigenvalues over a large range. For $(KCl)_5$, the peak near the high end of the fast-rate eigenvalue distribution increases in amplitude and decreases in linewidth. In contrast, for Ar_9 this peak broadens as temperature decreases. We also note that in Ar_9 the leading edge of the fast-rate band shifts by roughly one decade as temperatures increases from 4 K to 28 K, where in $(KCl)_5$ this downward shift of the leading edge is not nearly as marked.

IV. PES BASIN STRUCTURES

As noted in Paper I, only one ''monotonic sequence basin'' exists on the $(KCl)_5$ PES. The Ar_9 PES has only two such basins, with the secondary basin being only one transition step deep, and containing only one minimum not in the primary basin. Not surprisingly, the monotonic sequence construction of basins is not likely to give significant insight on the subdomains in which a small cluster can equilibrate on relatively short time scales. Nevertheless, at any temperature one may find regions on the PES in which passage among minima occurs readily within some chosen time scale, or equivalently, above a chosen rate threshold. These regions form kinetically defined basins on the PES, in the sense that the cluster will tend to be confined to this region on the chosen time scale. As temperature increases, raising more transition rates above the rate threshold, these basins merge so that the effective number of regions on the PES decreases, and the new region incorporates a larger number of minima. At a sufficiently high temperature (if the cluster does not evaporate), all minima will belong to one basin, and

the cluster can be said to be in a liquid state on this time scale. At this temperature, the whole of the PES is accessible to the cluster on a suitable time scale.

Basins defined in this manner are analogous to the groups or ''clusters'' of multivariate data formed by clustering algorithms. These algorithms use a similarity function or metric to characterize the similarity or distance, respectively, between two members of the data set.[30,31] Our approach uses the interconversion rate of neighboring structures as a measure of kinetic proximity on the PES to determine when two minima merge into a common basin. This procedure reveals a treelike hierarchy—which we refer to as a *connectivity tree*—that is valuable in describing the effects of PES structure on kinetics, and is often used to describe the PES in the theory of spin glasses.[32,33] In general, it can be used to examine the ruggedness of the PES in terms of kinetic barriers and to pinpoint the temperature of effective ergodicity breaking, as well as the subregions into which the PES is broken during this process.

Becker and Karplus[23] have given a detailed discussion of a similar approach, couched in terms of graph theory. In their approach, the hierarchical tree diagram is termed a *canonical disconnectivity graph*. They point out that microcanonical metrics—such as the barrier height threshold they have used to produce topological disconnectivity graphs, and the similar ''energy lid'' of Sibani *et al.*[34]—are ideal for examining the roughness of the PES topography, whereas canonical disconnectivity graphs, analogous to those used in this paper, illustrate the separation of the kinetics into basins at any given temperature. They note that choosing a particular discrete spacing ΔT of hierarchical temperature levels in the graph illustrates the existence and connectivity of basins on a particular scale, measured by the number of minima comprising the average basin. They further note that as the level spacing becomes continuous ($\Delta T \rightarrow 0$), the disconnectivity graph is a chart of the local connectivity of minima. For small systems, few hierarchical levels will exist, and the number of mergers is necessarily small. Choosing a continuous temperature spacing is then more suitable for systems such as $(KCl)_5$ and Ar_9, in the sense that we can see in detail the mergers of individual basins of minima, which are relatively more important on a small PES than they would be on a larger surface.

We perform our analysis on both $(KCl)_5$ and Ar_9 by placing each minimum in its own basin at $T=0$, and using the following merge criterion: when transition rate $k^{j\rightarrow i}$ and the reverse rate $k^{i\rightarrow j}$ both exceed a given threshold k_{crit}, the basin containing minimum i and the basin containing minimum j are merged into one basin. Any other members of the respective basins of minima i and j at lower temperatures also become members of the new common basin. This process always produces basins that are mutually disjoint sets of minima, since each minimum belongs to one and only one basin at a given temperature.

We illustrate the method for $(KCl)_5$ using the MB($\eta_P = 0.1$)-N model. Figure 9(a) gives the resulting tree diagram. For reasons explained below, we use the rate threshold $k_{\mathrm{crit}} = 10^9$/s for the merge criterion, corresponding to 500 000 time steps in the $(KCl)_5$ simulations. At low temperatures, the dominant merge scenario is a single minimum joining a pre-existing basin of one or more minima. Five especially stable basins form that exist over large temperature ranges; these are the last basins formed by addition of a single minimum. The minima belonging to each of these basins are listed in Table II.

These basins can be discerned in Fig. 2 of Paper I by observing groups of monotonic sequences separated from other sequences by large barrier heights. Basin members share a degree of geometric similarity, particularly in Basins I and II (see Fig. 1 of Paper 1). Basin I members are nonplanar objects, in the sense that they have no extended planar features, as most members of other basins do. Basin II contains three minima, all corresponding to two-dimensional structures (rectangle, decagon, and bent-rectangle). This basin is well separated from the rest of the PES; the bent-rectangle (minimum 9) connects only to the rectangle and the global minimum, and the decagon (minimum 8) connects only to the rectangle.

We selected the rate threshold k_{crit} so that temperatures at which two critical mergers occur would roughly coincide with corresponding discontinuities[35] in the relative rms bond length fluctuation δ of Eq. (13). The first discontinuity is due to the onset of rearrangements among Basin I minima, and so coincides with the merger of the global minimum with other Basin I minima. The second discontinuity is due to the exploration of minima in Basin II in addition to Basin I and hence coincides with the merger of Basins I and II. This second temperature is at the lower bound of the coexistence region between solidlike and higher-energy minima, and is evident as a change of slope in the caloric curve.

It is important to note that there is no fundamental choice of k_{crit} for a given system. We use it in this work as an adjustable parameter to match merger temperatures observed in the particular MD study of Ref. 32. In general, longer MD simulations tend to yield lower merger temperatures. Merger temperatures also decrease for connectivity trees when k_{crit} is decreased; for $k_{\mathrm{crit}} = 10^6$/s, the temperatures of the merger of the global minimum of $(KCl)_5$ into Basin I and the merger of Basins I and II are half of their values when $k_{\mathrm{crit}} = 10^9$/s. The simulation length plays the same role as does k_{crit} in the connectivity tree; both set the time scale within which large bond length fluctuations must occur. Hence, for mergers to occur at the same temperatures in both simulation and in the connectivity tree, k_{crit} should be increased as the simulation length increases.

Basins III–V consist of structures that are best described as combinations of two planar features, or a planar and/or a ring feature. Minima in these basins commonly feature a pair of like-charged ions straddling a site that would normally be occupied by just one ion of that type. Minimum 22, the highest-energy minimum found, is essentially a collapsed version of minimum 6. Being the only ''amorphous'' conformation of $(KCl)_5$, it has an irregular geometry and C_1 symmetry. However, it merges into Basin V at a temperature well below that at which the five principal basins are established. This is not necessarily surprising, since the potential barrier between high-energy minima tends to be small, and at

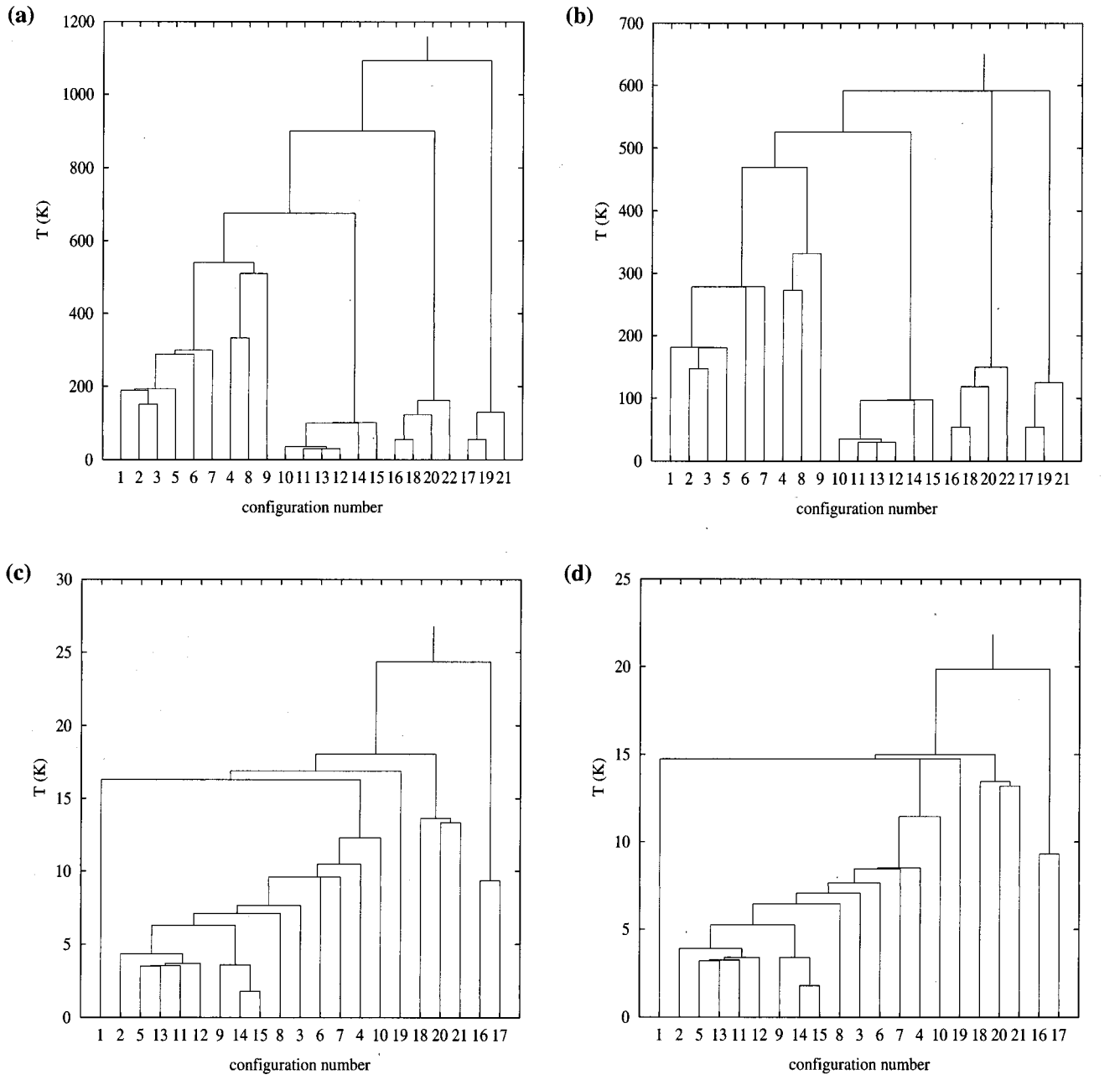

FIG. 9. The kinetic connectivity tree diagrams obtained for: (a) $(KCl)_5$, using the MB($\eta_P=0.1$)-N and (b) H-H models with $k_{crit}=10^9$/s; Ar_9, using the (c) MB($\eta_P=0.1$)/S-N and (d) models with $k_{crit}=2\times10^{10}$/s.

a sufficiently high energy the relation of structural similarity to kinetic accessibility can be expected to break down.

Figure 9(b) shows how the connectivity tree changes when the simple H-H model is used. Using the same k_{crit}, we obtain the same principal basins as we did for MB($\eta_P=0.1$)-N. In short, the differences between the models are quantitative, not qualitative. In both models, the minima merge in the same sequence. The most significant differences occur at high temperature, where the H-H model mergers occur at significantly lower temperatures than those of MB($\eta_P=0.1$)-N. While the merger involving minimum 1 (the first discontinuity in the δ) occurs at approximately the same temperature, the merger of Basins I and II now occurs at a lower temperature. According to the H-H model, ergodicity on the k_{crit} time scale can occur at 600 K, compared to the much higher ergodicity threshold of 1000 K predicted by MB($\eta_P=0.1$)-N. The relative temperature ranges over

TABLE II. Members of the five main basins of $(KCl)_5$.

Basin	Minima
I	1, 2, 3, 5, 6, 7
II	4, 8, 9
III	10, 11, 12, 13, 14, 15
IV	17, 19, 21
V	16, 18, 20, 22

which particular basins coexist have also changed. For example, the principal basins of H-H coexist over a 100 K range, but the MB($\eta_P=0.1$)-N model shortens this region to less than half the range, due to a lower-temperature merger of Basins I and II. In general, models that yield longer relaxation constants tend to expand the temperature scale of the connectivity tree, since the longer relaxation times are due to lowered transition rates, and hence greater dwell times in particular minima or basins.

We also applied the clustering technique to Ar_9 using the MB($\eta_P=0.1$)/S-N model. We have set $k_{crit}=2\times10^{10}$/s so that the merger of minimum 1 occurs approximately at the discontinuity temperature $T_D^{Ar_9}=16$ K set in Sec. III B. As observed for $(KCl)_5$, merger temperatures are sensitive to the choice of k_{crit}, decreasing by roughly half of their values when k_{crit} is decreased by a factor of 1000 to $k_{crit}=2\times10^7$/s. The resulting tree diagram in Fig. 9(c) illustrates why δ has only one discontinuity. Minimum 1 is kinetically isolated below 16 K. At this temperature, minimum 1 merges with another basin which already contains minima 2–15. Within the new super-basin, the system can explore most of the PES, and can visit all minima that have appreciable occupation probabilities at pre-dissociation temperatures. Hence this one merger allows the atoms of Ar_9 to sharply increase their rearrangement possibilities, resulting in an abrupt rise in δ. Subsequent mergers do not promote fluctuations significantly larger than those already possible in the super-basin formed at $T_D^{Ar_9}$.

The basin structure of Ar_9 is more complex than that of $(KCl)_5$. The global minimum forms its own basin (Basin I) up to the ''coexistence'' temperature near $T_D^{Ar_9}$. There is a steadily growing Basin II that is initially comprised of two sub-basins: Basin II-a, including minima 2, 5, 11, 12, and 13, and Basin II-b, including minima 9, 14, and 15. As temperature increases, Basin II grows to encompass the remaining low-energy minima in the order 8, 3, 7, 6, 4. Minima 10 and 19 are then included at higher temperatures, with minimum 19 merging above $T_D^{Ar_9}$. Two more basins appear, comprised of the highest-energy minima: Basin III, comprised of minima 18, 20, and 21, and Basin IV, containing minima 16 and 17.

Applying the clustering algorithm using the H-H model [Fig. 9(d)], and again using $k_{crit}=2\times10^{10}$/s, we found that mergers occurred at temperatures only slightly lower than in the MB($\eta_P=0.1$)/S-N case. This decrease is consistent with the small difference between harmonic and numerically approximated $Z^\dagger$ values in Ar_9, since exchanging one $Z^\dagger$ model for the other type makes little difference in transition rate expressions.

V. CONCLUSIONS

In general, using MB($\eta_P=0.1$) models to approximate Z^M, and numerical or Taylor-approximated models for $Z^\dagger$, yields master equations whose solutions give the best agreement with simulated relaxation. For Ar_9, the η_P variant of the MB model class, although important for modeling P^{eq}, is not significantly better in modeling the kinetic results than the models with no free parameters.

For $(KCl)_5$, the capabilities of a model to describe both equilibrium and kinetic features of relaxation appear to be correlated. For Ar_9, however, the correlation is somewhat weaker, with some reasonable models of P^{eq} performing quite poorly for relaxation, and vice versa. In the case of Ar_9, there are several cases in which the FTSV/H-N and MB/S-N models are the closest to simulation results. Of these models, MB/S-N is competitive with the MB($\eta_P=0.1$)/S-N model at all temperatures. At high temperatures, FTSV/H-N results suffer due to poor predictions equilibrium populations, and is not a reliable model for general use.

Given an accurate Z^M model, the best model for $Z^\dagger$ is a numerical or Taylor approximation; the harmonic approximation tends to yield low-frequency relaxation modes that are faster than the corresponding modes observed in simulation. For $(KCl)_5$, the $Z^\dagger$ model choice makes a large difference in the RRKM rates and, subsequently, the relaxation predictions. Notably, the H-N makes a large improvement over the relaxation rates given by the H-H model. For Ar_9, on the other hand, this model choice makes less difference in the relaxation rates. These observations are supported by comparisons made in Paper I of the calculated $Z^\dagger$ rates using both types of model, as well as direct explorations of the $(KCl)_5$ and Ar_9 surfaces in the region of transition-states, which showed an average tendency of the transition-state normal modes to be stiffer than their harmonic approximations. While this trend is marked in $(KCl)_5$, it is much less so in Ar_9.

For temperatures high enough for the clusters to exhibit liquidlike behavior, our model predictions tend to break down. Also, the harmonic $Z^\dagger$ models, which typically give higher rate constants, appear to yield better agreement with the MD results at these temperatures. However, it is likely that RRKM theory will break down at this point, due the the increasing importance of transition states with more than one negative normal mode, and possibly due to a breakdown in the Markovian dynamics assumption. To show that the good agreement of harmonic $Z^\dagger$ models at high temperature (or at fast rate) is fortuitous, we note that at low temperatures, RRKM rate expressions are more trustworthy, and smaller anharmonic effects mean that models can accurately model Z^M. Since the results for these models, used with a Taylor-approximated or numerical $Z^\dagger$, are closer to simulation values than those with harmonic $Z^\dagger$ approximations, we conclude that the numerical $Z^\dagger$ values are more accurate, and that harmonic $Z^\dagger$ values tend to be too high. In any case, we note that low-temperature behavior is the most important to model correctly, since it is in this temperature region where the final outcome of relaxation (on some chosen time scale) will be significantly localized, necessitating accurate model predictions. Also, since the dynamics at low temperature are rate limited by transition barriers, low-temperature relaxation will be a greater determinant of whether a PES is a structure-seeker or a glass-former.

Our detailed examination of $P_i(t)$ for select minima i using both master equation techniques and simulation has proved successful in identifying important transition-state

pathways to equilibrium, and for studying the rate-limitingeffects of the potential well connectivity. We also examined the evolution of the average quenched energy $\langle E_q(t)\rangle$ for both $(KCl)_5$ and Ar_9, which provides a simple, comprehensive picture of relaxation behavior, allowing an additional comparison between simulation and the master equation. We also derived spectral information from $\langle E_q(t)\rangle$ which we could compare directly to the information about master equation eigenmodes. Although the spectral resolution of the simulation data was limited, we were able to identify the most important relaxation modes in these data, and make correspondences between the important modes and the master equation eigenvalues. Our study of the $\langle E_q(t)\rangle$ spectrum forms a quantitative basis for comparing simulation data to master equation results, and will be valuable in future work, where we will test the accuracy of master equations constructed from statistical samples of the PES.

We also employed a data ''clustering'' technique to determine the kinetic connectivity of minima on using RRKM transition rates. Our technique identified a hierarchy of basins on the PES of a given system, in which the system may be confined on a given time scale. For $(KCl)_5$, in particular, minima within stable basins are not only dynamically linked, but geometrically related as well. We note that the clustering of minima into basins is somewhat insensitive to choice of model; specifically, the order in which smaller basins merge to form super-basins is robust. However, the temperatures at which these mergers occur can vary significantly from model to model for the same value of k_{crit}.

Our kinetic clustering description of the PES is useful for smaller systems where basin structure, as strictly defined by monotonic sequences, is either absent, as in the case of $(KCl)_5$, or misleading, as noted[36] for the PES of the polypeptide bead model studied by Elmaci *et al.*[11] where two low-lying minima, connected by a high saddle, would be considered in the monotonic sequence picture to be part of the same basin. We also note that our kinetic connectivity picture is more relevant than the topographic basin description, since it directly describes the dynamic evolution of clusters and polymers. Our clustering method relates the topographic connectivity of minima to their kinetic connectivity, and is an important preliminary investigation into how the topography of the energy surface is related to the kinetic zones of localization, and how time scales for exploring successively larger zones emerge from the topography.

With suitably chosen partition function models, the master equation successfully replicates results from molecular dynamics, providing a reassuring basis for extending the approach to larger systems where the potential surfaces and master equations can only be represented by statistical samples. The next stage in our investigation will be to compare such statistical-sample master equations with full master equations for clusters slightly larger than $(KCl)_5$ and Ar_9.

Note added in proof. Despite the thoroughness of our PES search in Paper I, an ongoing study[37] has recently discovered new minima and saddles for $(KCl)_5$. In total, 35 minima and 116 saddles were found, 82 of which are nondegenerate. This study also employs EF searches, but starts with configurations found on a shorter-range, shielded Coulomb PES[4] and reoptimizes them using the unshielded Coulomb potential. As found in earlier studies[38–42] on the effects of varying the range of the interatomic potential, the number of stationary points generally increases with decreasing interaction range. Hence the initial set of stationary points on a shorter-range PES provides a better initial coverage of the longer-range PES, allowing the inclusion of PES regions that might not otherwise be found by EF searches alone. This approach may prove to be a valuable tool in future PES explorations.

Since our PES search effort failed to find a number of stationary points, we tested the relevance of the new points to equilibrium and kinetic properties, and find that our results are robust with respect to the addition of these points. First, the new minima are essentially irrelevant to the kinetics; indeed, none of them were ever visited in our MD simulations at temperatures below the dissociation region. These minima are higher in energy than those in the original set by an extremely large energy gap of 0.0497 eV/ion, more than twice the size of any other energy gap between minima, indicating that the role played by these new minima is negligible in both equilibrium and kinetic studies at subdissociation temperatures.

Second, only nondegenerate transitions will be relevant to the kinetics, so we only need to compare the effect of adding an additional 32 nondegenerate transition states to the 50 already in the original set. Moreover, since the new minima can be neglected, only transitions between two minima in the original set will be kinetically significant. There are only 13 such transition states in the new data. Of these, only two have saddle energies lying in the low-to-intermediate range of the $(KCl)_5$ saddle energy distribution, with the rest lying at the high end of the distribution with severely Boltzmann-attenuated occupation probabilities. The lower-energy of these two transitions (SA72) connects minima 2 and 4, while the other (SA105) connects minima 4 and 9. Since these minima are all relatively low in energy, these two saddles are the most likely of the 13 to cause a deviation from our results obtained on the original PES sample.

Upon examination of relaxation profiles starting with $P_{19}(t=0)=1$ at $T=400$, 520, and 800 K, we found that including SA72 in the PES sample caused negligible perturbations in P_1^{eq} profiles (as well as P_4^{eq}, P_8^{eq}, and P_{19}^{eq}) and in the $\langle E_q(t)\rangle$ profile at each temperature. Furthermore, adding SA105 or even all 13 saddles to the data set did not cause any significant change. We therefore conclude that our ''complete'' sample of the $(KCl)_5$ PES was, indeed, sufficiently complete for dynamical study of $(KCl)_5$.

ACKNOWLEDGMENT

This research was supported by Grant No. CHE-9414258 from the National Science Foundation.

[1] P. J. Steinhardt, D. R. Nelson, and M. Ronchetti, Phys. Rev. B **28**, 784 (1983).
[2] K. D. Ball, R. S. Berry, R. E. Kunz, F. Li, A. Proykova, and D. J. Wales, Science **271**, 963 (1996).
[3] M. Amini and R. W. Hockney, J. Non-Cryst. Solids **31**, 447 (1979); M. Amini, D. Fincham, and R. W. Hockney, J. Phys. C **12**, 4707 (1979).

[4] J. P. Rose and R. S. Berry, J. Chem. Phys. **98**, 3262 (1993).
[5] P. E. Leopold, M. Montal, and J. N. Onuchic, Proc. Natl. Acad. Sci. USA **89**, 8721 (1992).
[6] J. D. Bryngelson and P. G. Wolynes, Proc. Natl. Acad. Sci. USA **84**, 7524 (1987).
[7] J. N. Onuchic, P. G. Wolynes, Z. Luthey-Schulten, and N. D. Socci, Proc. Natl. Acad. Sci. USA **92**, 3626 (1995).
[8] J. D. Bryngelson, J. N. Onuchic, N. D. Socci, and P. G. Wolynes, Proteins: Struct., Funct., Genet. **21**, 167 (1995).
[9] P. G. Wolynes, J. N. Onuchic, and D. Thirumalai, Science **267**, 1619 (1995).
[10] N. D. Socci, J. N. Onuchic, and P. G. Wolynes, J. Chem. Phys. **104**, 5860 (1996).
[11] R. S. Berry, N. Elmaci, J. P. Rose, and B. Vekhter, Proc. Natl. Acad. Sci. USA **94**, 9520 (1997).
[12] K. D. Ball and R. S. Berry, J. Chem. Phys. **109**, 8541 (1998), preceding article.
[13] R. E. Kunz and R. S. Berry, J. Chem. Phys. **103**, 1904 (1995).
[14] R. S. Berry and R. E. Kunz, Phys. Rev. Lett. **74**, 3951 (1995).
[15] R. E. Kunz, R. S. Berry, and T. Astakhova, Surf. Rev. Lett. **3**, 307 (1996).
[16] G. U. Nienhaus, J. D. Muller, B. H. McMahon, and H. Frauenfelder, Physica D **107**, 297 (1997).
[17] J. P. K. Doye and D. Wales, J. Chem. Phys. **105**, 8428 (1996).
[18] R. E. Kunz, P. Blaudeck, K. H. Hoffmann, and R. S. Berry, J. Chem. Phys. **108**, 2576 (1998).
[19] N. G. van Kampen, *Stochastic Processes in Physics and Chemistry* (North-Holland, Amsterdam, 1981).
[20] M. Cieplak, M. Henkel, J. Karbowski, and J. R. Banavar, Phys. Rev. Lett. **80**, 3654 (1998).
[21] J. Wang, J. Onuchic, and P. Wolynes, Phys. Rev. Lett. **76**, 4861 (1996).
[22] A. Fernández and G. Appignanesi, Phys. Rev. Lett. **78**, 2668 (1997).
[23] O. M. Becker and M. Karplus, J. Chem. Phys. **106**, 1495 (1997).
[24] R. Czerminski and R. Elber, Proc. Natl. Acad. Sci. USA **86**, 6963 (1989).
[25] R. Czerminski and R. Elber, J. Chem. Phys. **92**, 5580 (1990).
[26] P. J. Robinson and K. A. Holbrook, *Unimolecular Reactions* (Wiley-Interscience, London, 1972).
[27] R. G. Gilbert and S. C. Smith, *Theory of Unimolecular and Recombination Reactions* (Blackwell Scientific, Oxford, 1990).
[28] B. Vekhter, K. D. Ball, J. Rose, and R. S. Berry, J. Chem. Phys. **106**, 4644 (1997).
[29] T. L. Beck, J. Jellinek, and R. S. Berry, J. Chem. Phys. **87**, 545 (1987).
[30] H. C. Romesburg, *Cluster Analysis for Researchers* (Lifetime Learning Publications, Belmont, CA, 1994).
[31] S. Miyamoto, *Fuzzy Sets in Information Retrieval and Cluster Analysis* (Kluwer Academic, Dordrecht, 1990).
[32] R. Rammal, G. Toulouse, and M. Virasoro, Rev. Mod. Phys. **58**, 765 (1986).
[33] K. Binder and A. P. Young, Rev. Mod. Phys. **58**, 801 (1986).
[34] P. Sibani, J. C. Schön, P. Salamon, and J. O. Andersson, Europhys. Lett. **22**, 479 (1993).
[35] J. P. Rose and R. S. Berry, J. Chem. Phys. **96**, 517 (1992).
[36] N. Elmaci, unpublished results.
[37] M. C. Nguyen, K. D. Ball, and R. S. Berry (unpublished).
[38] P. A. Braier, R. S. Berry, and D. J. Wales, J. Chem. Phys. **93**, 8745 (1990).
[39] J. P. K. Doye, D. J. Wales, and R. S. Berry, J. Chem. Phys. **103**, 4234 (1995).
[40] D. T. Mainz and R. S. Berry, Mol. Phys. **88**, 709 (1996).
[41] J. P. K. Doye and D. J. Wales, J. Phys. B **29**, 4859 (1996).
[42] J. P. K. Doye and D. J. Wales, J. Chem. Soc., Faraday Trans. **93**, 4233 (1997).